pH and Cation Effects on the Properties of Parallel Pyrimidine Motif DNA Triplexes†

Naoki Sugimoto,*,‡,§ Peng Wu,‡ Hideyuki Hara,§ and Yasunori Kawamoto§

High Technology Research Center and Department of Chemistry, Faculty of Science and Engineering, Konan University, 8-9-1 Okamoto, Higashinada-ku, Kobe 658-8501, Japan

Received April 3, 2001; Revised Manuscript Received June 1, 2001

ABSTRACT: The effects of cytosine protonation and various cations on the properties of parallel pyrimidine motif DNA triplexes were intensively investigated and characterized by several different techniques, such as circular dichroism (CD) conformation, ultraviolet (UV) melting, differential scanning calorimetry (DSC) thermal denaturation, and surface plasmon resonance (SPR) real-time dynamics. The comparative CD spectra of the triplex and the corresponding homoduplexes showed that the negative peak at ∼218 nm would be the eigenpeak of the Hoogsteen paired strand, and moreover, the formation pathway of a triplex was significantly pH-dependent and fell into three groups: under acidic conditions, the triplex is formed by a one-step docking, under near physiological conditions, the Watson−Crick duplex is first structured and then accepts the Hoogsteen third strand into its major groove, and under basic conditions, the triplex is not formed. The pH-dependent thermodynamics of the global triplex, the Watson−Crick antiparallel duplex, and the Crick−Hoogsteen parallel duplex were comparatively discussed for the first time. These data revealed that the thermodynamic stabilities of the Watson−Crick−Hoogsteen triplex and the Crick−Hoogsteen duplex would be strongly dependent on cytosine protonation, but a low-pH environment somewhat destabilized the Watson−Crick duplex. The binding energy of triplex formation would be different from the unfolding energy of triplex melting under acidic conditions due to the disparity in the pathway between the formation and unfolding of a triplex. Real-time dynamic measurements showed that the association and dissociation rate constants of a duplex-to-triplex formation are $(1.98 \pm 0.24) \times 10^3$ M^{-1} s^{-1} and $(4.09 \pm 0.96) \times 10^{-4}$ s^{-1} at 20 °C and pH 6.0, respectively. The formation energy of the duplex-to-triplex transition derived from SPR measurements was in agreement with the unfolding energy of the free Hoogsteen paired duplex derived from UV measurements. The calorimetric enthalpies of the triplex-to-duplex-to-single transition were 39.3 and 75.3 kcal/mol under near physiological conditions (pH 7.0), respectively, which were underestimated relative to the van't Hoff enthalpies. In addition, the effects of various cations, ionic strength, mixed-valent cations, and the position of the $C^+ \times G \cdot C$ triplets on the thermodynamics of the triplexes were addressed under near physiological conditions. The interaction of metal ions with the triplexes clearly depended on the type and ionic strength of the cations, and the efficiency with which the cations stabilized the global triplex was in the order $Mg^{2+} > Mn^{2+} > Ca^{2+} > Ba^{2+} \gg Na^+$. These observations would be useful for the design of triplex-forming oligonucleotides for antigene drugs and therapeutic purposes.

Nucleic acids have the potential to form not only double helix structures (*1*) but also triple and G-quadruple helix structures (*2*, *3*). Despite a lack of direct evidence for the tertiary structure of nucleic acids in vivo, the presence of H-DNA was often considered to regulate gene transcription (*4*, *5*) and the sequence-specific DNA ligands of the triplex-forming oligonucleotides (TFOs) have been proven to target specific mutations in somatic cells of adult mice after intraperitoneal injection (*6*, *7*). Moreover, the oligonucleotide-directed triplexes were extensively applied for sequence-specific modification to recognize the double-stranded nucleic acid targets or the cleavage of nucleic acids (*8*−*10*). These potential gene-targeted therapeutic and biotechnological applications have provoked considerable interest in triplex formation and stability (*11*−*18*). In general, triplexes can be subdivided into intermolecular and intramolecular complexes and have parallel and antiparallel structures according to the composition and orientation of the third strand. Parallel motif triplexes require protonation at N3 of the cytosine residues and are stabilized by low pH and high ionic strength (*13*, *19*−*23*). Surprisingly, the pH dependence of the thermodynamic characterization for a parallel motif triplex, except in a few reports (*13*, *24*, *25*), has been lacking. Typically, only melting temperatures are measured. Furthermore, the protonation effect on the thermodynamic properties of the homoduplexes in a triplex, especially the Crick−Hoogsteen parallel duplex, has not yet been clearly understood.

† This work was supported in part by Grants-in-Aid from the Ministry of Education, Science, Sports and Culture, Japan, and a grant from the "Research for the Future" program of the Japan Society for the Promotion of Science to N.S.

* To whom correspondence should be addressed. Phone: +81-78-435-2497. Fax: +81-78-435-2539. E-mail: sugimoto@konan-u.ac.jp.

‡ High Technology Research Center.

§ Department of Chemistry, Faculty of Science and Engineering.

10.1021/bi010666l CCC: $20.00
Published on Web 07/10/2001

Metal ions play an important role in biologically stabilizing the structures of nucleic acids and could have promoted the evolution of nucleic acid structures (*26*−*28*). Although the cation effects on triplex formation have been investigated by several chemical methods (*11*, *29*, *30*, *31*), the cation dependence of the thermodynamic property and stability for triplex formation has not been well characterized under near physiological conditions. To apply triplexes as the therapeutic antigene drugs for artificial control of gene expression in vivo, a more detailed investigation remains to be addressed.

In the present study, we first characterized the CD[1] spectra of the Hoogsteen paired strand by comparing the conformational differences between the global Watson−Crick−Hoogsteen triplex, the Watson−Crick antiparallel duplex, and the Crick−Hoogsteen parallel duplex, and then divided the formation pathway of a parallel pyrimidine motif triplex into three groups over a wide pH range. The protonation effects on the thermodynamic properties of the global triplex, the Watson−Crick duplex, and the Crick−Hoogsteen duplex were investigated and extensively compared for the first time. The dynamic binding ability of the Hoogsteen strand to the host duplex was further evaluated by surface plasmon resonance (SPR). In the end, we also focused on the influence of various cations, ionic strength, mixed-valent cations, and the position of the $C^+ \times G \cdot C$ triplets on the triplex stability under near physiological conditions.

MATERIALS AND METHODS

DNA Oligonucleotide Preparation and Purification. Various 12-mer DNA oligonucleotides, 5′-TCTTCTCTTTCT-3′ (PyW1), 5′-AGAAAGAGAAGA-3′ (PuC1), 5′-TCTTTCTCTTCT-3′ (PyH1), 5′-TTTCCTTCTTCT-3′ (PyW2), 5′-AGAAGAAGGAAA-3′ (PuC2), 5′-TCTTCTTCCCTTT-3′ (PyH2), 5′-TTTCCCTTTCTT-3′ (PyW3), 5′-AAGAAAGGGAAA-3′ (PuC3), and 5′-TTCTTTCCCTTT-3′ (PyH3), were synthesized on a solid support using the standard phosphoramidite chemistry process on an Applied Biosystems model 391 DNA synthesizer and were purified by HPLC with Wakosil-II 5C18RS cartridges after deblocking operations. These oligonucleotides were further purified and desalted with Sep-Pak C-18 cartridges. The final purity of the oligonucleotides was confirmed by HPLC. The oligonucleotides were then aliquoted in various buffer solutions for CD, UV, DSC, and SPR experiments. Single-strand concentrations were determined by measuring the absorbance (260 nm) at a high temperature. The different DNA strands were mixed in equimolar amounts, and the total species concentrations were estimated by averaging the extinction coefficients of the single strands (*32*).

UV Measurements. UV thermal scans were carried out on Hitachi U-3200 and U-3210 spectrophotometers equipped with a Hitachi SPR-10 thermoprogrammer and temperature probe. The water condensation on the cuvette exterior in the low-temperature range can be avoided by flushing with a constant stream of dry nitrogen. Melting curves were collected by UV absorbance (260 nm) as a function of temperature. The heating rates were fixed at 0.5 or 1.0 °C/min according to the cuvette path lengths and strand concentrations. Prior to the sample experiments, all samples were first annealed and degassed by heating the sample cuvette to 95 °C for 20 min and then cooled to room temperature. The samples were allowed to stabilize for ∼10 min at the beginning temperature of each heating−cooling cycle.

CD Measurements. CD spectra were recorded on a Jasco J-820 spectropolarimeter equipped with a PTC-423L temperature controller. DNA samples were equilibrated for ∼30 min prior to each scan. For each sample, at least six spectrum scans were accumulated over the wavelength range of 200−350 nm and the temperature range of 0−90 °C in a 0.1 cm path length cell at a scanning rate of 10 nm/min. The scan of the buffer alone was subtracted from the average scan for each sample. CD spectra were collected in units of millidegrees versus wavelength, normalized to the total species concentrations, and then converted to $\epsilon_L - \epsilon_R$ versus wavelength (*33*). The cell holding chamber was flushed with a constant stream of dry nitrogen to avoid water condensation on the cell exterior.

DSC Measurements. DSC measurements were performed on a MicroCal VP-DSC microcalorimeter. The calorimeter was calibrated by using pure paraffin hydrocarbons sealed in a steel capillary tube with an internal heater for a calibration pulse. Prior to scanning, the buffer and samples were vacuum degassed. Buffer versus buffer cells was scanned to determine the baseline of the instrumental variation between the cells of the calorimeters before DNA samples versus buffer scans were collected. For each DNA sample, six scans were collected from 0 to 90 °C at a rate of 60 °C/h. The resulting sample versus buffer scans collected for each sample were averaged, and the buffer versus buffer baseline was subtracted and then normalized by the strand concentration and the sample volume to obtain the excess heat capacity, ΔC_P, versus temperature, T, profiles. The transition temperature was determined by the peak height maximum of the baseline-corrected ΔC_P vs T profiles, and the calorimetric enthalpy was calculated from the integration area (*11*, *17*, *21*, *33*, *34*).

SPR Measurements. A BIAcore biosensor was used for SPR measurements. Streptavidin was immobilized onto a sensor chip (CM5) using amine coupling chemistry at a flow rate of 5 μL/min in HBS buffer (10 mM HEPES, 150 mM NaCl, 3.4 mM EDTA, and 0.005% P20 surfactant). Thirty μL of streptavidin was injected at 400 μg/mL in 10 mM sodium acetate (pH 5.0), followed by the reaction of excess activated groups with 1 M ethanolamine hydrochloride (pH 8.5) to give a response of ∼3600 response units (RUs). The biotinylated PuC1 (Bt-PuC1) was injected at a concentration of 5 μM until ∼400 RUs were captured by the streptavidin surface. The same amount of PyW1 was injected to form a W−C duplex with the biotinylated ODN. After being extensively washed and reaching equilibration, PyH1 was then injected over the immobilized PyW1·PuC1 duplex surface to form a W−C−H triplex. All experiments were

[1] Abbreviations: UV, ultraviolet; CD, circular dichroism; DSC, differential scanning calorimetry; SPR, surface plasmon resonance; HPLC, high-performance liquid chromatography; T_m, maximum temperature of the derivative absorbance vs temperature curves (dA/dT vs T); W−C duplex, Watson−Crick duplex with the antiparallel pyrimidine−purine paired double helix; C−H duplex, Crick−Hoogsteen duplex with the parallel purine−pyrimidine paired double helix; W−C−H triplex, Watson−Crick−Hoogsteen triplex with the pyrimidine×purine·pyrimidine paired triple helix, where × indicates the Hoogsteen paired strand with the parallel deoxyribose−phosphate backbone and · indicates the Watson−Crick paired strand with the antiparallel deoxyribose−phosphate backbone.

carried out at 20 °C and at a flow rate of 15 μL/min in running buffer (10 mM $MgCl_2$/50 mM MES, pH 6.0). The chip surface was regenerated with 30 μL of HCl (0.01 M), followed by an injection of PyW1 to renew the immobilized duplex surface prior to each experiment cycle.

pH Dependence of Thermodynamic Analysis. Unless otherwise specified, the thermodynamic parameters of a triplex association/dissociation reaction were determined by UV melting measurements. Within our experimental range, the unfolding of the triplex-stranded DNAs is strongly dependent on the pH values of the solution medium and falls into three different groups (see the text below).

(1) Under acidic conditions (pH ≤ 6.5), the global triplex unfolding proceeds in a monophasic triplex-to-coil collapse (*12*, *35*, *36*, *37*, *38*)

$$S_WS_CS_H \rightleftharpoons S_W + S_C + S_H$$

and the equilibrium constant, K_T, can be written as

$$K_T = \frac{[S_WS_CS_H]}{[S_W][S_C][S_H]} = \frac{1-\alpha_T}{{\alpha_T}^3}\frac{9}{{C_T}^2} = \exp\left(\frac{-\Delta H_T + T\Delta S_T}{RT}\right) \quad (1)$$

where $S_WS_CS_H$ represents the Watson−Crick−Hoogsteen triplex, ΔH_T and ΔS_T are the van't Hoff enthalpy and entropy of triplex formation, respectively, α_T is the molar fraction of the coiled strands in the structured triplex form, and C_T is the total species concentration. At the maximum temperature of the derivative absorbance vs temperature curves (dA/dT vs T), α_T should be equal to ∼0.63 (*37*); therefore, the van't Hoff equation can be written as

$${T_m}^{-1} = \frac{2R}{\Delta H_T}\ln\frac{C_T}{3.65} + \frac{\Delta S_T}{\Delta H_T} \quad (2)$$

(2) Under near physiological conditions (pH 7.0−7.5), the global triplex unfolding proceeds in a biphasic triplex-to-duplex-to-single transition and can be deconvoluted into two coupled subtransitions, a Hoogsteen transition and a Watson−Crick transition (*11*, *14*, *25*, *35*, *39*−*42*)

$$S_WS_CS_H \rightleftharpoons S_WS_C + S_H \rightleftharpoons S_W + S_C + S_H$$

and the corresponding equilibrium constants, K_H and K_{WC}, can be given by, respectively

$$K_H = \frac{[S_WS_CS_H]}{[S_WS_C][S_H]} = \frac{1-\alpha_H}{\alpha_H(\alpha_H-\alpha_{WC})}\frac{3}{C_T} = \exp\left(\frac{-\Delta H_H + T\Delta S_H}{RT}\right) \quad (3)$$

$$K_{WC} = \frac{[S_WS_C]}{[S_W][S_C]} = \frac{\alpha_H-\alpha_{WC}}{{\alpha_{WC}}^2}\frac{3}{C_T} = \exp\left(\frac{-\Delta H_{WC} + T\Delta S_{WC}}{RT}\right) \quad (4)$$

where S_WS_C represents the Watson−Crick duplex, ΔH_H, ΔS_H, ΔH_{WC}, and ΔS_{WC} are the van't Hoff enthalpies and entropies for the Hoogsteen transition and Watson−Crick transition, respectively, α_H is the molar fraction of the Hoogsteen strand in the structured triplex state for the Hoogsteen transition, and α_{WC} is the molar fraction of the Watson−Crick duplex in the corresponding coiled state for the Watson−Crick transition (*12*, *13*, *43*). Although the two transitions may overlap each other in a certain range, this cross-effect can be nearly neglected at the melting temperatures (*13*, *25*), and the values of α_{WC} and α_H at which the derivative absorbance vs temperature curves reach their maxima should be ∼0.42 and ∼0.50, respectively (*41*, *42*). Thus, the van't Hoff equations can be simplified by

$${T_H}^{-1} = \frac{R}{\Delta H_H}\ln\frac{C_T}{10.35} + \frac{\Delta S_H}{\Delta H_H} \quad (5)$$

$${T_{WC}}^{-1} = \frac{R}{\Delta H_{WC}}\ln\frac{C_T}{6} + \frac{\Delta S_{WC}}{\Delta H_{WC}} \quad (6)$$

(3) Under basic conditions (pH ≥ 8.0), the triplex strand is not formed and the complex unfolding merely includes a monophasic duplex-to-coil transition. That is

$$S_WS_C + S_H \rightleftharpoons S_W + S_C + S_H$$

and the equilibrium constant, K_D, can be given by

$$K_D = \frac{[S_WS_C][S_H]}{[S_W][S_C][S_H]} = \frac{1-\alpha_D}{{\alpha_D}^2}\frac{3}{C_T} = \exp\left(\frac{-\Delta H_D + T\Delta S_D}{RT}\right) \quad (7)$$

where ΔH_D and ΔS_D are the van't Hoff enthalpy and entropy of duplex formation in the 1:1:1 mixture of the three strands, respectively, and α_D is the molar fraction of the coiled strands in the structured duplex form. For this case, the maximum temperature should take place at $\alpha_D = 0.50$ (*44*, *46*), and therefore, the van't Hoff equation can be written as

$${T_D}^{-1} = \frac{R}{\Delta H_D}\ln\frac{C_T}{6} + \frac{\Delta S_D}{\Delta H_D} \quad (8)$$

Although more complicated models would be suggested for intramolecular triplex formation (*19*, *21*), the thermodynamic parameters of intermolecular triplex formation derived from the $1/T_m$ vs $\ln(C_T/n)$ plots can provide a reasonable approximation within the allowed range of deviation (*25*). For the Watson−Crick antiparallel duplex and the Crick−Hoogsteen parallel duplex, the thermodynamic parameters of duplex formation can be directly estimated by the van't Hoff equation (*44*, *46*):

$${T_m}^{-1} = \frac{R}{\Delta H}\ln\frac{C_T}{4} + \frac{\Delta S}{\Delta H} \quad (9)$$

It should be emphasized that to avoid possible errors in estimating the thermodynamic parameters due to the difference between the maximum temperature and the melting midpoint temperature (*47*), the van't Hoff enthalpies and entropies of the antiparallel and parallel duplexes were still determined by using the maximum temperature of the derivative absorbance versus temperature curves.

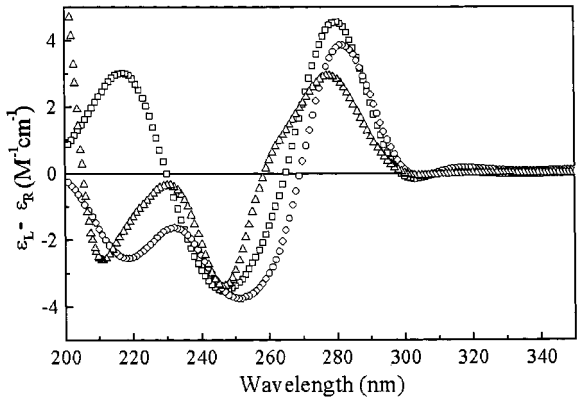

FIGURE 1: Representative CD spectra of the PyH1×PuC1•PyW1 triplex (○), the PyW1•PuC1 antiparallel duplex (□), and the PuC1×PyH1 parallel duplex (△) in 10 mM Mg^{2+} buffer. All spectra were collected at 0 °C and in a total species concentration of 70 μM.

Kinetic Analysis for Binding of the Hoogsteen Strand to the Watson−Crick Duplex. A one-to-one reaction model is assumed for the kinetic analysis. The association sensorgram is the net result of the association reaction and dissociation reaction, and therefore, the apparent association rate of the duplex-to-triplex reaction can be described by

$$\frac{dR}{dt} = k_a C_H (R_{max} - R) - k_d R \qquad (10)$$

where R is the response at time t, R_{max} is the maximum response, k_a and k_d are the association and dissociation rate constants, respectively, and C_H is the Hoogsteen strand concentration. A plot of dR/dt vs R gives a line with a slope of $-(k_a C_H + k_d)$, the so-called apparent association constant, k_{obs}. By measuring k_{obs} at different Hoogsteen strand concentrations, k_a is thus obtained as the resulting slope of a k_{obs} vs C_H plot (*48*).

The dissociation rate constant, k_d, can be directly estimated by the dissociation sensorgram according to

$$\frac{dR}{dt} = -k_d R \qquad (11)$$

and a plot of $\ln(R/R_{max})$ vs t yields a line with a slope of $-k_d$. The resulting k_d is obtained by averaging the values derived from different Hoogsteen strand concentrations (*49, 50*). The equilibrium affinity constant and free energy are further evaluated by the equations $K_a = k_a/k_d$ and $\Delta G = -RT \ln K_a$, respectively.

RESULTS AND DISCUSSION

Eigenpeak of the CD Spectra for the Hoogsteen Paired Strand. The representative CD spectra of the PyH1×PuC1•PyW1 triplex, the PyW1•PuC1 antiparallel duplex, and the PuC1×PyH1 parallel duplex at 0 °C are shown in Figure 1. The direct conformation comparison of the triplex and host W−C duplex reveals that the two structures are characterized by strong positive peaks at ∼282 nm and negative peaks at ∼251 nm, but the peaks at ∼218 nm are just opposite each other in the vectorial direction. In contrast, the CD spectra of the C−H duplex are remarkably similar to those of the triplex, differing only in the intensity of the peaks and a slight blue shift in the peak position. Given the structural features of the parallel triplexes by high-resolution NMR spectroscopy and X-ray crystallography (*14, 51−53*), the negative peak at ∼218 nm would be regarded as the eigenpeak of the CD spectra for the Hoogsteen paired strand, which suggests that the Hoogsteen strand would harbor rightly in the center of the major groove of the host W−C duplex to form the parallel triplex, and meanwhile, the addition of the Hoogsteen strand needs only small readjustments of the host W−C duplex to adapt this conformational change without significantly distorting the duplex structure. Analogous observations have been reported for the previous CD studies (*42, 43, 54, 55*).

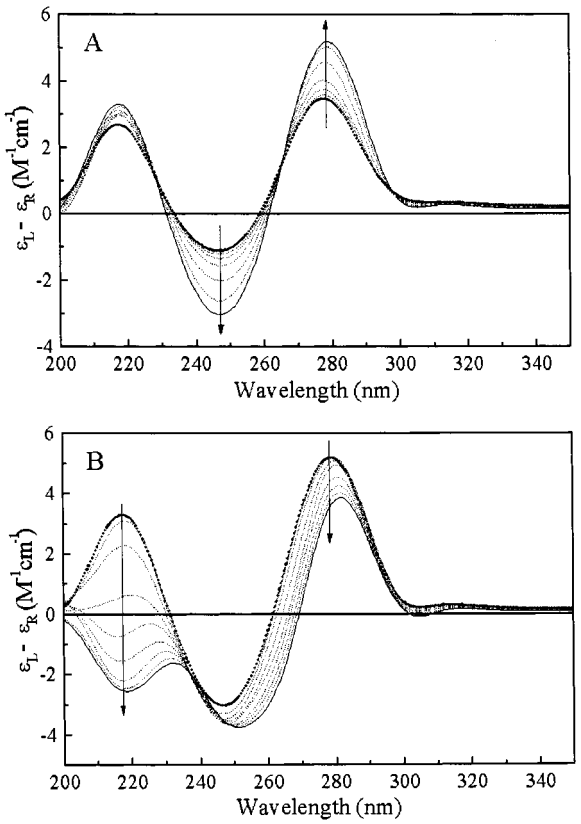

FIGURE 2: CD spectra of PyH1×PuC1•PyW1 triplex formation as a function of temperature in 10 mM Mg^{2+}/50 mM HEPES buffer (pH 7.0). To clarify the conformational changes in the two sequential transitions, the entire temperature range was divided into two parts: (A) Watson−Crick transition region (40−70 °C) and (B) Hoogsteen transition region (0−40 °C). The arrow indicates the change from high temperature to low temperature at an interval decrease of 5 °C. All spectra were collected in a total species concentration of 70 μM.

Conformational Changes and Formation Pathway of the Triplex at Various pH Values. The CD spectra of PyH1×PuC1•PyW1 triplex formation in 10 mM Mg^{2+}/50 mM HEPES buffer (pH 7.0) are shown in Figure 2. The spectra demonstrate that triplex formation under near physiological conditions can be divided into two sequential processes: the Watson−Crick base-pairing (high-temperature region) and the Hoogsteen base-pairing (low-temperature region). In the Watson−Crick transition region, with decreasing temperature, the CD spectra show the typical feature of duplex association, in which the first positive peak and the first negative peak (hereafter numbered consecutively from long wavelength to short wavelength) are remarkably enhanced

in magnitude, and two isoelliptic points occur at ~228 and ~265 nm. When the temperature continues to decrease, the association process enters into the Hoogsteen transition region. In this region, the second positive peak is dramatically reduced in magnitude, and finally, the entire peak disappears and turns into a negative peak, which reaches a minimum when the Hoogsteen strand completely associates with the host W−C duplex into the structured W−C−H triplex. In contrast, the first positive peak is reduced in magnitude while the first negative peak is raised nearly to the same magnitude as the first positive peak. Meanwhile, the position of these two peaks is accompanied by a clear red shift. Alternatively, the CD spectra in the wavelength range of 250−282 nm seem to move downward to the long wavelength nearly in a parallel pattern. Moreover, only one isoelliptic point at ~236 nm may reflect that this transition is from duplex to triplex. Anyway, these observations reveal that the W−C duplex is first structured and then accepts the Hoogsteen third strand into its major groove to form the triplex.

The CD spectra under acidic or basic conditions are obviously different from those under near physiological conditions. At low pH, with decreasing temperature, the magnitudes of all the peaks are simultaneously enhanced and no positive peak is observed at ~218 nm. Moreover, the shift in peak position does not take place at ~218 and ~282 nm (see the Supporting Information). This implies that the triplex would be formed by a one-step docking under acidic conditions (*55*). At high pH, the CD spectra have no negative peak at ~218 nm and present a typical characteristic of Watson−Crick duplex formation along with the temperature change (see the Supporting Information), which suggests that the triplex is not formed under this condition. The pH-dependent CD spectra of the complex formation of PuC1 and PyW1 and/or PyH1 strands as a function of temperature are extracted at two characteristic wavelengths, ~218 and ~282 nm, as shown in Figure 3. These spectra further confirm that the formation of DNA complexes in the 1:1:1 mixture of the three strands falls into three different groups: at pH ≤ 6.5, the triplex is formed in a single-to-triplex docking, at pH 7.0−7.5, the triplex is formed in a single-to-duplex-to-triplex docking; and at pH ≥ 8.0, the triplex is not formed and only the duplex is formed in a single-to-duplex docking.

Protonation Effect on the Thermodynamics of the W−C−H Triplex, W−C Duplex, and C−H Duplex. UV melting experiments show that, at low pH, the unfolding of DNA complexes is a monophasic transition and has a high hyperchromicity, at near physiological pH, the unfolding is a biphasic transition, and at high pH, the unfolding is still a monophasic transition but has a low hyperchromicity (see the Supporting Information). These observations are quite consistent with CD measurements and imply that the triplex association/dissociation transition is a reversible process. To gain comprehensive insight into the possible effect of protonation on the different base pairs and backbones, the pH-dependent thermodynamics of the PyH1×PuC1•PyW1 triplex, the PyW1•PuC1 antiparallel duplex, and the PuC1×PyH1 parallel duplex were also investigated under identical conditions, as shown in Figure 4. These data reveal that the thermodynamic stabilities of the PyH1×PuC1•PyW1 triplex and the PuC1×PyH1 duplex are clearly dependent on pH and are enhanced with decreasing pH, while the thermodynamic stability of the PyW1•PuC1 duplex has a slight reduction with decreasing pH. This suggests that protonation has two opposite effects: one is to promote the stabilities of the W−C−H triplex and C−H duplex, and the other is to decrease the stability of the W−C duplex. It should be emphasized that the structural forms of the PuC1 and PyH1 paired strand at various pH values were further confirmed by CD spectra (see the Supporting Information). The results show that the PuC1 and PyH1 paired strand is a parallel duplex (i.e., PuC1×PyH1) at low pH but rearranges into the antiparallel duplex with bulges at pH 7.0 or higher, which is in good agreement with the previous study (*54*).

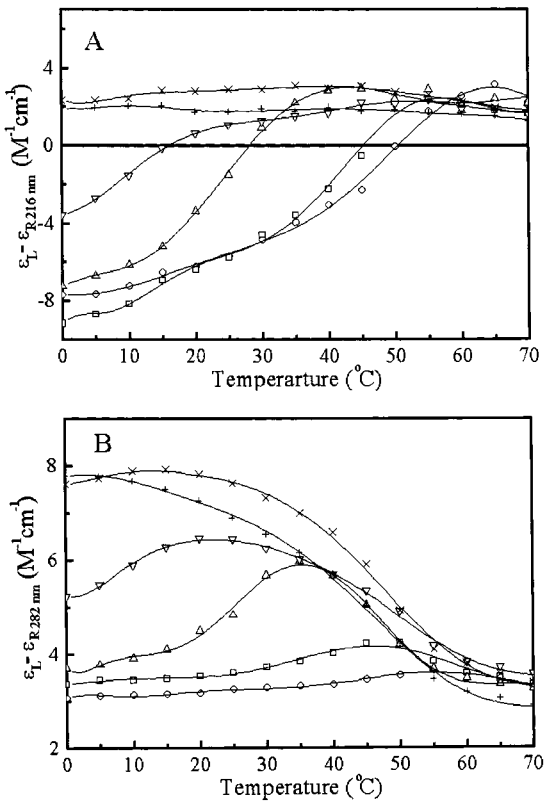

FIGURE 3: pH-dependent CD spectra for complex formation of PuC1 and PyW1 and/or PyH1 strands as a function of temperature at (A) ~218 nm and (B) ~282 nm: pH 5.5 (○), pH 6.0 (□), pH 7.0 (△), pH 7.5 (▽), pH 8.0 (+), pH 9.0 (×).

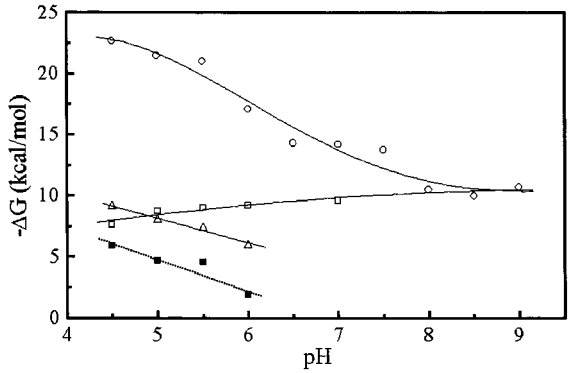

FIGURE 4: pH-dependent free energies of the PyH1×PuC1•PyW1 triplex (○), the PyW1•PuC1 antiparallel duplex (□), and the PuC1×PyH1 parallel duplex (△) and $\Delta\Delta G = \Delta G$(PyH1×PuC1•PyW1) − ΔG(PyW1•PuC1) − ΔG(PuC1×PyH1) (■). All experiments were performed in 10 mM Mg^{2+} containing a 50 mM concentration of the following buffers: Tris−acetate buffer (pH 4.5−5.0), MES buffer (pH 5.5−7.0), and Tris−HCl (pH 7.5−9.0).

Table 1: Comparative Kinetics and Thermodynamics for PyH1×PuC1•PyW1 Triplex Formation at 20 °C and pH 6.0[a]

SPR measurements[b]			UV measurements[c]		
k_a (10^3 M^{-1} s^{-1})	k_d (10^{-4} s^{-1})	ΔG (kcal/mol)	ΔG(W−C−H) (kcal/mol)	ΔG(W−C) (kcal/mol)	ΔG(C−H) (kcal/mol)
1.98 ± 0.24	4.09 ± 0.96	−8.96 ± 0.12	−24.58 ± 0.50	−13.39 ± 0.16	−8.97 ± 0.06

[a] All experiments were performed in 10 mM Mg^{2+}/50 mM MES buffer (pH 6.0). [b] k_a, k_d, and ΔG are the association rate constant, the dissociation rate constant, and the free energy change from the W−C duplex to the W−C−H triplex, respectively. [c] ΔG(W−C−H), ΔG(W−C), and ΔG(C−H) are the free energies of the W−C−H triplex, the free Watson−Crick antiparallel duplex, and the free Crick−Hoogsteen parallel duplex, respectively.

In addition, Figure 4 also reveals the fact that the free energy of the global triplex is much smaller than the sum of the free energies of the free Watson−Crick duplex and free Crick−Hoogsteen duplex under acidic conditions, that is, ΔG(W−C−H) < ΔG(W−C) + ΔG(C−H), which suggests that a larger energy would be required to disrupt the W−C−H triplex compared to individually disrupting the W−C duplex and C−H duplex. Alternatively, the triplex is a more stable complex than expected, and its unfolding would be the one-step collapse of the global molecule under acidic conditions. This observation is slightly different from the unfolding mechanism proposed by other labs (*13*, *55*). The possible interpretation is that the $d(C^+T)_n \times d(AG)_n \cdot d(CT)_n$ triplex has two structural forms, the ~90% 3′ dangling triplex and the ~10% 5′ dangling triplex, at low pH (*13*, *22*, *23*), and a small amount of the unstable 5′ dangling triplex would be first denatured. However, under our experimental conditions the PyH1×PuC1•PyW1 triplex has only one form.

Anyway, the pH-dependent thermodynamics of triplex formation has been reported only infrequently. The thermodynamic properties of the Hoogsteen paired strand were merely estimated by using the difference in the thermodynamic parameters between the global triplex and its host W−C duplex (*37*), that is, ΔG(C−H) = ΔG(W−C−H) − ΔG(W−C). It should be emphasized that the thermodynamic stability of the Hoogsteen paired strand derived in this way was generally overestimated, at least in our experimental range. Furthermore, our results imply that parallel triplex formation at low pH may have three pathways but its unfolding is merely a one-step collapse as follows:

$$S_W + S_C + S_H \rightleftharpoons S_W S_C S_H \quad \text{(i)}$$

$$S_W S_C + S_H \rightarrow S_W S_C S_H \quad \text{(ii)}$$

$$S_W + S_C S_H \rightarrow S_W S_C S_H \quad \text{(iii)}$$

Dynamic Detection of Triplex Formation. Figure 5 shows a typical series of SPR sensorgrams for binding of PyH1 to the PyW1•PuC1 duplex to form the PyH1×PuC1•PyW1 triplex at 20 °C in 10 mM $MgCl_2$/50 mM MES buffer (pH 6.0). The association rate constant and the dissociation rate constant are determined to be (1.98 ± 0.24) × 10^3 M^{-1} s^{-1} and (4.09 ± 0.96) × 10^{-4} s^{-1}, respectively, which are quite consistent with previous reports (*24*, *48*, *49*, *50*, *56*). To gain further insight into the equilibrium affinity ability and thermodynamic properties of triplex formation, the kinetic data and thermodynamic data are directly compared in Table 1. The results show that the binding energy of PyH1 to the PyW1•PuC1 duplex derived from kinetic measurements is remarkably consistent with the unfolding energy of the free PuC1×PyH1 duplex derived from thermodynamic measurements. This reflects the formation of the Hoogsteen paired strand being independent of the structural forms of the host strands. As a result, we concluded that the formation energy of a triplex would be different from its unfolding energy under acidic conditions due to the disparity in the pathway between the formation and unfolding of a triplex (see the text above). This case is very similar to a high hysteresis between the formation and unfolding of a parallel triplex (*56*).

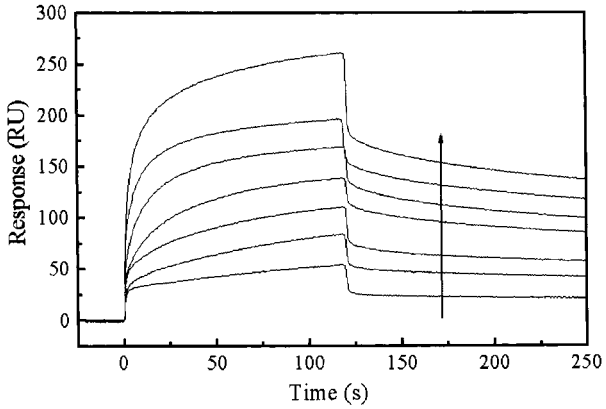

FIGURE 5: SPR sensorgram of binding of the PyH1 strand to the target PyW1•PuC1 duplex to form the PyH1×PuC1•PyW1 triplex at 20 °C and pH 6.0 (10 mM $MgCl_2$/50 mM MES buffer). The arrow indicates the increase in the PyH1 strand concentration (0.5, 1.0, 2.5, 5.0, 10.0, 20.0, and 40.0 μM).

Thermodynamic Comparison between Spectroscopy and Calorimetry Measurements. DSC, as an alternative method, has been applied more and more extensively to determine the thermodynamic parameters of oligonucleotides. DSC experiments for the PyH1×PuC1•PyW1 triplex thermal denaturation were carried out at a concentration of 60 μM in 10 mM $MnCl_2$/50 mM HEPES buffer (pH 7.0) (see the Supporting Information). The results show that the triplex unfolding was a biphasic transition from the viewpoint of excess heat capacity under near physiological conditions, in agreement with UV and CD measurements. The calorimetric enthalpy can be estimated by a cubic progressive baseline and the general assumption of $\Delta\Delta C_P = 0$ [where $\Delta\Delta C_P$ = ΔC_P(pre-transition) − ΔC_P(post-transition)] (*17*, *21*, *33*, *34*, *57*). The calorimetric enthalpies for the Hoogsteen transition and Watson−Crick transition are 39.3 and 75.3 kcal/mol, while the corresponding van't Hoff enthalpies are 59.8 and 102.2 kcal/mol under identical conditions, respectively. Such a discrepancy in the two enthalpy sets for the oligomeric triplexes has been observed by other labs, and in general, the calorimetric enthalpy was smaller than the van't Hoff enthalpy (*11*, *21*, *34*, *48*). Similarly, clear differences in the thermodynamic enthalpy derived from spectroscopy and calorimetry measurements have been observed in duplexes (*33*, *58*) and G-quadruplexes (*59*).

The difference between the van't Hoff enthalpy and calorimetric enthalpy appears to be a general problem that has been recently addressed by several labs (*21, 33, 48, 58*−*62*), all with slightly different conclusions and different emphases. Thermodynamics derived from UV measurements is model-dependent. The usual interpretation is that the helix-to-coil unfolding would be a partial two-state transition (*58, 60, 61*) and the difference in hydration between the structured groups and the coiled groups would result in a heat capacity increase (*44, 48, 62*). However, several observations argued against this explanation. The DSC transition profile showed that the two peaks for the Hoogsteen transition and Watson−Crick transition are clearly symmetric (see the Supporting Information), which confirms the validity of the two-state approximation within our experimental range. On the other hand, the transition temperatures derived from DSC measurements are very close to the maximum temperatures derived from UV measurements, which implies that the change of heat capacity in the spectroscopy analysis can be neglected for short triplex formation. These observations are in good agreement with the recent study on the triplex energetics (*25*). In contrast, thermodynamics derived from DSC measurements is considered to be model independent. Nevertheless, this method still implies the general assumption that the difference in excess heat capacity between the native and denatured states, $\Delta\Delta C_P$, is taken as zero (*11, 17, 21, 34, 48*). Considering that the calorimetric enthalpy is directly determined by excess heat capacity as a function of temperature, a change in excess heat capacity of various transition states (the structured triplex, the duplex and Hoogsteen strand, and the coiled strands) would be a dominant factor for the discrepancy between the van't Hoff enthalpy and calorimetric enthalpy. This viewpoint is further supported by recent studies (*59, 60*) in which the 100% disparity between the two enthalpies could be canceled when $\Delta\Delta C_P \neq 0$ was considered progressively (*59*). Although the changes in excess heat capacity of the pre-transition and post-transition states were suggested to be temperature-dependent and the more appreciable $\Delta\Delta C_P$ set was put forward to improve the calorimetric enthalpy (*59, 60*), it does become very difficult to determine the differences in excess heat capacity of each state, especially the intermediate state (the coexisting state of the duplex and Hoogsteen strand) due to the slight overlap between the Hoogsteen transition and Watson−Crick transition. Moreover, the different baseline constructions in the calorimetry analysis would give rise to some discrepancy in the resulting calorimetric enthalpy (*40, 59*), but it still lacks an unambiguous rule to assign the DSC baseline under the current conditions.

Effects of Ionic Strength and Mixed-Valent Cations on Triplex Stability. The stability of a triple helix structure can be influenced by the ionic strength and mixture of monovalent and divalent cations (*11, 13, 17, 21, 25, 31*). We investigated the effect of the Na^+ concentration on the PyH1×PuC1·PyW1 triplex stability, where the Na^+ concentrations were changed from 10 mM to 2 M and the total species concentrations were changed over ~100-fold (data not shown). The results show that when both the Na^+ concentrations and the strand concentrations are low, the melting temperatures of the Hoogsteen transition are too small to be determined, but this case cannot be observed when the Na^+ concentrations are high while the strand concentrations are still low. Although the melting temperatures of the Hoogsteen transition and Watson−Crick transition increase with increasing Na^+ concentrations, the stability of the Hoogsteen paired strand more strongly depends on the ionic strength than does that of the Watson−Crick paired duplex (data not shown).

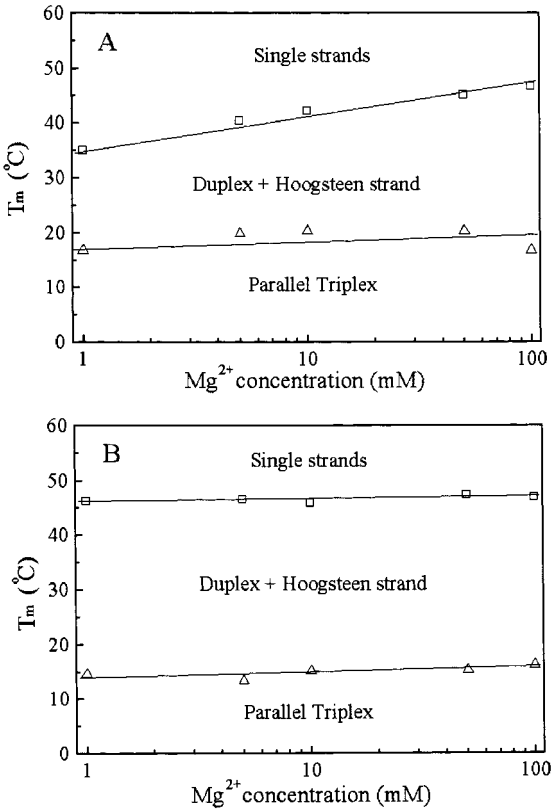

FIGURE 6: Mg^{2+} concentration dependence of the melting temperature of the PyH1×PuC1·PyW1 triplex for the Hoogsteen transition (△) and Watson−Crick transition (□). All experiments were carried out in 50 mM HEPES buffer (pH 7.0) in (A) the absence of 1 M Na^+ and (B) the presence of 1 M Na^+. The data were determined in a total species concentration of 6 μM.

To gain insight into the effect of the mixed-valent cations on the triplex stability, the melting experiments for the PyH1×PuC1·PyW1 triplex were carried out in the absence or presence of 1 M Na^+ containing various Mg^{2+} concentrations (pH 7.0), as shown in Figure 6. The results show that the melting temperature of the Watson−Crick transition is more dependent on the Mg^{2+} concentration than that of the Hoogsteen transition in the absence of Na^+. The possible interpretation is that Mg^{2+} presents a site-specific binding and is predisposed to bind to phosphate groups (*63*), which may favor stabilizing the duplex more than the third strand. In contrast, the melting temperature of the Watson−Crick transition becomes nearly Mg^{2+}-concentration-independent in the presence of 1 M Na^+, and the melting temperature of the Hoogsteen transition in the presence of Na^+ is clearly lower than that in the absence of Na^+. This result may be attributed to the competition between the two different valent cations when binding to the triplex. Since Na^+ is typically non-site-specific and binds to phosphates and bases, under such a high Na^+ concentration, Na^+ almost shields the negative charges where Mg^{2+} would bind, which results in the insensitivity of the W−C duplex stability on Mg^+ and reduces the stability of the Hoogsteen paired strand. These

Table 2: Thermodynamic Parameters for Parallel Triplex Formation in Various Cations

	Hoogsteen transition[b]				Watson−Crick transition[b]			
cation[a]	ΔH_H (kcal/mol)	ΔS_H [cal/(mol K)]	ΔG_{H37} (kcal/mol)	T_H[c] (°C)	ΔH_{WC} (kcal/mol)	ΔS_{WC} [cal/(mol K)]	ΔG_{WC37} (kcal/mol)	T_{WC}[c] (°C)
PyW1• PuC1× PyH1 triplex: d(TCTTCTCTTTCT)/d(AGAAAGAGAAGA)/d(TC TTTCTCTTCT)								
Na^+	42.7 ± 2.4	120.4 ± 8.2	5.36 ± 0.15	24.7	66.3 ± 2.8	180.8 ± 8.7	10.23 ± 0.12	53.9
Mg^{2+}	71.7 ± 5.7	215.3 ± 19.2	4.92 ± 0.26	27.7	99.5 ± 4.6	288.1 ± 14.5	10.08 ± 0.09	47.8
Mn^{2+}	59.9 ± 4.0	175.8 ± 13.4	5.32 ± 0.20	28.2	102.2 ± 4.2	298.7 ± 13.4	9.51 ± 0.06	45.7
Ca^{2+}	52.5 ± 1.8	153.4 ± 6.1	4.90 ± 0.10	24.6	96.4 ± 4.9	282.1 ± 15.6	8.85 ± 0.05	44.0
Ba^{2+}	57.3 ± 0.8	170.1 ± 2.8	4.57 ± 0.05	23.7	89.1 ± 5.1	260.6 ± 17.7	8.26 ± 0.39	42.3
PyW2• PuC2×PyH2 triplex: d(TTTCCTTCTTCT)/d(AGAA GAAGGAAA)/d(TCTTCTTC CCTTT)								
Na^+	nd[d]	nd	nd	nd	nd	nd	nd	nd
Mg^{2+}	53.1 ± 3.6	158.3 ± 12.6	4.04 ± 0.29	19.8	103.0 ± 3.4	298.7 ± 10.7	10.40 ± 0.08	48.0
Mn^{2+}	49.9 ± 1.7	147.0 ± 5.4	4.32 ± 0.02	20.4	98.7 ± 2.0	286.8 ± 5.8	9.84 ± 0.18	46.6
Ca^{2+}	51.3 ± 3.7	152.4 ± 13.0	4.06 ± 0.32	19.4	89.5 ± 3.2	259.1 ± 10.1	9.15 ± 0.05	45.4
Ba^{2+}	58.4 ± 1.6	178.1 ± 5.0	3.19 ± 0.06	17.3	87.9 ± 3.8	255.2 ± 12.2	8.89 ± 0.01	44.0
PyW3•PuC3 ×PyH3 triplex: d(TTTCCCTTTCTT)/d(AAGA AAGGGAAA)/d(TTCTTTCC CTTT)								
Na^+	58.0 ± 2.5	176.6 ± 8.6	3.56 ± 0.21	17.5	82.7 ± 3.7	230.5 ± 11.4	11.15 ± 0.15	54.5
Mg^{2+}	51.9 ± 4.1	156.1 ± 12.5	3.47 ± 0.25	16.7	123.7 ± 4.9	363.1 ± 16.4	11.04 ± 0.20	48.2
Mn^{2+}	51.4 ± 5.2	154.2 ± 16.0	3.51 ± 0.19	16.9	106.8 ± 2.9	311.9 ± 9.2	10.08 ± 0.05	46.9
Ca^{2+}	51.6 ± 4.4	155.1 ± 13.1	3.38 ± 0.26	16.7	87.1 ± 5.1	250.8 ± 16.2	9.29 ± 0.08	46.3
Ba^{2+}	58.2 ± 4.6	181.3 ± 15.4	2.03 ± 0.20	11.8	86.4 ± 5.8	250.7 ± 18.3	8.68 ± 0.06	43.8

[a] All experiments were carried out in a buffer of 50 mM HEPES (pH 7.0) containing 1000 mM Na^+, 10 mM Mg^{2+}, 10 mM Mn^{2+}, 10 mM Ca^{2+}, and 10 mM Ba^{2+}, respectively. [b] The Hoogsteen transition is a triplex-to-duplex unfolding process in the low-temperature range, and the Watson−Crick transition is a duplex-to-single unfolding process in the high-temperature range. The thermodynamic stability of the global triplex can be evaluated by the sum of the free energies of the two transitions (*40, 69*). [c] T_H and T_{WC} are the melting temperatures of the Hoogsteen transition and Watson−Crick transition in 10^{-4} M total species concentration, respectively. [d] Not determined.

insights are indirectly supported by a footprinting assay (*11*) and quantitative affinity cleavage titration (*64*). Moreover, the competition and displacement of the mixed-valent cations in stabilizing the oligomeric structure have also been observed in the RNA tertiary structure (*65*).

Cation Effect on the Thermodynamics of the Triplex. DNA is negatively charged and its stability is explicitly dependent on the countercations. We investigated the influence of various cations, such as an alkali metal (Na^+), alkaline-earth metals (Mg^{2+}, Ca^{2+}, and Ba^{2+}), and transition metals (Mn^{2+}, Co^{2+}, and Zn^{2+}), on the thermodynamic properties of PyH1×PuC1•PyW1, PyH2×PuC2•PyW2, and PyH3×PuC3•PyW3 triplexes at pH 7.0, as summarized in Table 2. Co^{2+} and Zn^{2+} were subject to slight and obvious aggregations within our experimental range, respectively; therefore, the data are not shown. Considering the possible effect of ionic environments on triplex formation and stability, all cations were investigated as their chloride salts and the divalent cations were kept at the same ionic strength.

The data in Table 2 show that the thermodynamic stability of a triplex is much greater with divalent cations than with monovalent cations, and almost a 100-fold concentration of Na^+ is required to stabilize the triplex as effectively as Mg^{2+} or Mn^{2+} (*27, 64*). This case may be related to the valence-specific cationic stability of the triple helix structure (*64*). In the series of Mg^{2+}, Mn^{2+}, Ca^{2+}, and Ba^{2+}, the W−C duplex stability in the triplex increases from left to right (i.e., $Mg^{2+} > Mn^{2+} > Ca^{2+} > Ba^{2+}$). This order is in good agreement with the ionic radii of the divalent cations ($r_{Mg^{2+}} = 0.66$ Å, $r_{Mn^{2+}} = 0.80$ Å, $r_{Ca^{2+}} = 0.99$ Å, and $r_{Ba^{2+}} = 1.34$ Å, ref *26*), which suggests that the divalent cations with a smaller radius may increase the affinity of the nucleotide alignment, resulting in enhancing the stability of the double helix structure. A very similar case has recently been reported for the RNA tertiary structure, in which the stabilizing ability of a monovalent cation to RNA depends on the ionic radius (*65*). Interestingly, the order of the divalent cations for stabilizing the W−C duplex in the triplex is consistent with that for stabilizing the free W−C duplex (data not shown), but differs somewhat from that for stabilizing the Hoogsteen paired strand. This implies that the interaction of divalent cations with the triplex may be different for the Watson−Crick duplex and the Hoogsteen paired strand; however, the divalent cations stabilize the global triplex in an order nearly identical to that for stabilizing the host W−C duplex due to the larger difference in free energy between the W−C duplex and the Hoogsteen paired strand.

The influence of divalent cations on the triple helices is rather complicated and not yet well understood. The results presented here show a slight difference from the cation effect on the intermolecular Pu×Pu•Py triplexes (*11, 31*). Since the protonation at N3 of Hoogsteen cytosine residues plays a key role in stabilizing the Py×Pu•Py triplex structure while the Pu×Pu•Py triplex does not require this precondition, the interaction of divalent cations with a triplex may be very different for the two classes of triplexes. It has been reported that Mg^{2+} is crucial for the formation of the Pu×Pu•Py triplexes but not for the formation of the Py×Pu•Py triplexes (*66*). Another possibility may be due to the differences in buffer species, pH value, and base sequences.

Effect of the Position of the C^+GC Triplet on Triplex Stability. It is generally thought that triplexes containing the C^+×G•C triplets are thermally more stable than those completely formed by the T×A•T triplets, but the relative position of the C^+×G•C triplets would affect the triplex stability (*19, 20, 40, 67, 68*). Interestingly, these investigations mostly focused on the intramolecular triplexes, and moreover, the effect of the position of the C^+GC triplets on the stability of the intermolecular triplexes has yet to be determined for the various cations under near physiological conditions. To extend these results, we herein compared the thermodynamic properties of PyH1×PuC1•PyW1, PyH2×

PuC2•PyW2, and PyH3×PuC3•PyW3, where all three triplexes have the same base compositions and differ only in that the C^+×G•C triplet in PyH1×PuC1•PyW1 is flanked by the T×A•T triplet, while PyH2×PuC2•PyW2 and PyH3×PuC3•PyW3 contain the adjacent two and three C^+×G•C triplets, respectively, as shown in Table 2.

Apparently, the adjacent placing of the C^+×G•C triplets does destabilize the Hoogsteen paired strand but somewhat favors stabilizing the W−C duplex, resulting in the destabilization of the global triplex complex under near physiological conditions. This inverse correlation of the thermodynamic stability between the Hoogsteen paired strand and the Watson−Crick paired strand is in good agreement with previous studies (*20, 69*). A further comparison in Table 2 reveals that the stability of the intermolecular triplexes is reduced as the adjacent number of C^+×G•C triplets increases for all cations investigated under near physiological conditions; that is, the stable order of triplexes is PyH1×PuC1•PyW1 > PyH2×PuC2•PyW2 > PyH3×PuC3•PyW3. It is of particular interest that the degree of triplex destabilization also decreases with increasing adjacent number of C^+×G•C triplets. Alternatively, the difference in free energy of the Hoogsteen paired strand between PyH2×PuC2•PyW2 and PyH1×PuC1•PyW1 is larger than that between PyH3×PuC3•PyW3 and PyH2×PuC2•PyW2. A reduction of the triplex stability due to the adjacent placing of two C^+×G•C triplets can be attributed to changes of both favorable enthalpy and unfavorable entropy. But when the third C^+×G•C triplet is inserted into the adjacent C^+×G•C triplets, this reduction would come primarily from the conformational entropy change.

Although electrostatic repulsion of the adjacent C^+×G•C triplets has been attributed to a factor of triplex destabilization (*67*), the lower protonation of the cytosine residues in the adjacent C^+×G•C triplets would be more important. The possible interpretation is that the difference in free energy between the protonated and unprotonated C×G•C triplets would be significantly large (*19*) and a neutral pH environment merely results in the partial protonation of the cytosine residues in the Hoogsteen strand (*20*). Consequently, the protonation degree of a cytosine in the adjacent C^+×G•C triplets would be decreased by another cytosine due to the competition effect, resulting in a clear reduction in the thermodynamic stability of the Hoogsteen paired strand. This reflects the intrinsic protonation of the cytosine residues possibly being dependent on their nearest neighbors. These observations are supported by NMR measurements: the semiprotonation point of the cytosines in the adjacent C^+×G•C triplets is considerably smaller by 0.6 pH unit than that in the isolated C^+×G•C triplets (*20*), but when the cytosine residues are fully protonated, the adjacent placing of two cytosine residues has a slight or no effect on the triplex stability (*19*). These observations suggest that the design of TFOs should avoid the adjacent placing of multiple C^+×G•C triplets under physiological conditions to obtain stable TFOs for antigene drugs and therapeutic purposes.

SUPPORTING INFORMATION AVAILABLE

Five figures showing the CD spectra of the PyH1×PuC1•PyW1 triplex formation as a function of temperature at pH 4.0 and 9.0, the representative pH dependence of the PyH1×PuC1•PyW1 triplex unfolding, the pH-dependent CD spectra of the PuC1 and PyH1 paired strand at 0 °C, and the excess heat capacity vs temperature profile of the PyH1×PuC1•PyW1 triplex thermal denaturation. This material is available free of charge via the Internet at http://pubs.acs.org.

REFERENCES

1. Watson, J. D., and Crick, F. H. C. (1953) *Nature 171*, 737−738.
2. Felsenfeld, G., Davies, D. R., and Rich, A. (1957) *J. Am. Chem. Soc. 79*, 2023−2024.
3. Sen, D., and Gilbert, W. (1988) *Nature 334*, 364−366.
4. Cooney, M., Czernuszewicz, G., Postel, E. H., Flint, S. J., and Hogan, M. E. (1988) *Science 241*, 456−459.
5. Mirkin, S. M., Lyamichev, V. I., Drushlyak, K. N., Dobrynin, V. N., Filippov, S. A., and Frank-Kamenetskii, M. D. (1987) *Nature 330*, 495−497.
6. Vasquez, K. M., Wang, G., Havre, P. A., and Glazer, P. M. (1999) *Nucleic Acids Res. 27*, 1176−1181.
7. Vasquez, K. M., Narayanan, L., and Glazer, P. M. (2000) *Science 290*, 530−533.
8. Barre, F. X., Ait-Si−Ali, S., Giovannangeli, C., Luis, R., Robin, P., Pritchard, L. L., Hélène, C., and Harel-Bellan, A. (2000) *Proc. Natl. Acad. Sci. U.S.A. 97*, 3084−3088.
9. Maher, L. J., Dervan, P. B., and Wold, B. (1992) *Biochemistry 31*, 70−81.
10. Strobel, S. A., Doucette-Stamm, L. A., Riba, L., Housman, D. E., and Dervan, P. B. (1991) *Science 254*, 1639−1642.
11. Floris, R., Scaggiante, B., Manzini, G., Quadrifoglio, F., and Xodo, L. E. (1999) *Eur. J. Biochem. 260*, 801−809.
12. He, Y., Scaria, P. V., and Shafer, R. H. (1997) *Biopolymers 41*, 431−441.
13. Lavelle, L., and Fresco, J. R. (1995) *Nucleic Acids Res. 23*, 2692−2705.
14. Liu, K., Sasisekharan, V., Miles, H. T., and Raghunathan, G. (1996) *Biopolymers 39*, 573−589.
15. Moser, H. E., and Dervan, P. B. (1987) *Science 238*, 645−650.
16. Musso, M., Thomas, T., Shirahata, A., Sigal, L. H., van Dyke, M. W., and Thomas, T. J. (1997) *Biochemistry 36*, 1441−1449.
17. Plum, G. E., Park, Y. W., Singleton, S. F., Dervan, P. B., and Breslauer, K. J. (1990) *Proc. Natl. Acad. Sci. U.S.A. 87*, 9436−9440.
18. Sugimoto, N., Shintani, Y., Tanaka, A., and Sasaki, M. (1992) *Bull. Chem. Soc. Jpn. 65*, 535−540.
19. Asensio, J. L., Lane, A. N., Dhesi, J., Bergqvist, S., and Brown, T. (1998) *J. Mol. Biol. 275*, 811−822.
20. Leitner, D., Schröder, W., and Weisz, K. (2000) *Biochemistry 39*, 5886−5892.
21. Plum, G. E., and Breslauer, K. J. (1995) *J. Mol. Biol. 248*, 679−695.
22. Rajagopal, P., and Feigon, J. (1989) *Nature 339*, 637−640.
23. Rajagopal, P., and Feigon, J. (1989) *Biochemistry 28*, 7859−7870.
24. Singleton, S. F., and Dervan, P. B. (1992) *Biochemistry 31*, 10995−11003.
25. Mills, M., Arimondo, P. B., Lacroix, L., Garestier, T., Hélène, C., Klump, H. H., and Mergny, J. L. (1999) *J. Mol. Biol. 291*, 1035−1054.
26. Kazakov, S. A., and Hecht, S. M. (1994) in *Encyclopedia of Inorganic Chemistry* (King, R. B., Ed.) Vol. 5, pp 2697−2720, John Wiley & Sons Ltd., Chichester, U.K..
27. Nakano, S., Fujimoto, M., Hara, H., and Sugimoto, N. (1999) *Nucleic Acids Res. 27*, 2957−2965.
28. Patil, S. D., and Rhodes, D. G. (2000) *Nucleic Acids Res. 28*, 2439−2445.
29. Bernués, J., Beltrán, R., Casasnovas, J. M., and Azorín, F. (1990) *Nucleic Acids Res. 18*, 4067−4073.
30. Malkov, V. A., Voloshin, O. N., Soyfer, V. N., and Frank-Kamenetskii, M. D. (1993) *Nucleic Acids Res. 21*, 585−591.

31. Blume, S. W., Lebowitz, J., Zacharias, W., Guarcello, V., Mayfield, C. A., Ebbinghaus, S. W., Bates, P., Jones, D. E., Jr., Trent, J., Vigneswaran, N., and Miller, D. M. (1999) *Nucleic Acids Res. 27*, 695−702.
32. Richards, E. G. (1975) in *Handbook of Biochemistry and Molecular Biology: Nucleic Acids* (Fasman, G. D., Ed.) 3rd ed., Vol.1, p 597, CRC Press, Cleveland, OH.
33. Vallone, P. M., and Benight, A. S. (2000) *Biochemistry 39*, 7835−7846.
34. Völker, J., Botes, D. P., Lindsey, G. G., and Klump, H. H. (1993) *J. Mol. Biol. 230*, 1278−1290.
35. Xodo, L. E., Manzini, G., and Quadrifoglio, F. (1990) *Nucleic Acids Res. 18*, 3557−3564.
36. Thomas, T., and Thomas, T. J. (1993) *Biochemistry 32*, 14068−14074.
37. Pilch, D. S., Levenson, C., and Shafer, R. H. (1991) *Biochemistry 30*, 6081−6087.
38. Trapane, T. L., Hogrefe, R. I., Reynolds, M. A., Kan, L., and Ts'o, P. O. P. (1996) *Biochemistry 35*, 5495−5508.
39. Evertsz, E. M., Rippe, K., and Jovin, T. M. (1994) *Nucleic Acids Res. 22*, 3293−3303.
40. Scaria, P. V., and Shafer, R. H. (1996) *Biochemistry 35*, 10985−10994.
41. Xodo, L. E., Manzini, G., Quadrifoglio, F., van der Marel, G. A., and van Boom, J. H. (1991) *Nucleic Acids Res. 19*, 5625−5631.
42. Pilch, D. S., Brousseau, R., and Shafer, R. H. (1990) *Nucleic Acids Res. 18*, 5743−5750.
43. Manzini, G., Xodo, L. E., Gasparotto, D., Quadrifoglio, F., van der Marel, G. A., and van Boom, J. H. (1990) *J. Mol. Biol. 213*, 833−843.
44. Petersheim, M., and Turner, D. H. (1983) *Biochemistry 22*, 256−263.
45. Sugimoto, N., Nakano, M., and Nakano, S. (2000) *Biochemistry 39*, 11270−11281.
46. Ramsing, M. B., Rippe, K., and Jovin, T. M. (1989) *Biochemistry 28*, 9528−9535.
47. Tamura, A., and Privalov, P. L. (1997) *J. Mol. Biol. 273*, 1048−1060.
48. Asensio, J. L., Dosanjh, H. S., Jenkins, T. C., and Lane, A. N. (1998) *Biochemistry 37*, 15188−15198.
49. Bates, P. L., Dosanjh, H. S., Kumar, S., Jenkins, T. C., Laughton, C. A., and Neidle, S. (1995) *Nucleic Acids Res. 23*, 3627−3632.
50. Torigoe, H. (2001) *Biochemistry 40*, 1063−1069.
51. Bartley, J. P, Brown, T., and Lane, A. N. (1997) *Biochemistry 36*, 14502−14511.
52. Nunn, C. M., Trent, J. O., and Neidle, S. (1997) *FEBS Lett. 416*, 86−89.
53. Rhee, S., Han, Z. J., Liu, K., Miles, H. T., and Davies, D. R. (1999) *Biochemistry 38*, 16810−16815.
54. Liu, K., Miles, H. T., Frazier, J., and Sasisekharan, V. (1993) *Biochemistry 32*, 11802−11809.
55. Hashem, G. M., Wen, J. D., Do, Q., and Gray, D. M. (1999) *Nucleic Acids Res. 27*, 3371−3379.
56. Rougée, M., Faucon, B., Mergny, J. L., Barcelo, F., Giovannangeli, C., Garestier, T., and Hélène, C. (1992) *Biochemistry 31*, 9269−9278.
57. Völker, J., Osborne, S. E., Glick, G. D., and Breslauer, K. J. (1997) *Biochemistry 36*, 756−767.
58. Wu, P., and Sugimoto, N. (2000) *Nucleic Acids Res. 28*, 4762−4768.
59. Smirnov, I., and Shafer, R. H. (2000) *Biochemistry 39*, 1462−1468.
60. Jelesarov, I., Crane-Robinson, C., and Privalov, P. L. (1999) *J. Mol. Biol. 294*, 981−995.
61. Holbrook, J. A., Capp, M. W., Saecker, R. M., and Record, M. T., Jr. (1999) *Biochemistry 38*, 8409−8422.
62. Rouzina, I., and Bloomfield, V. A. (1999) *Biophys. J. 77*, 3242−3251.
63. Saenger, W. (1984) *Principles of Nucleic Acid Structure*, Springer-Verlag, New York.
64. Singleton, S. F., and Dervan, P. B. (1993) *Biochemistry 32*, 13171−13179.
65. Shiman, R., and Draper, D. E. (2000) *J. Mol. Biol. 302*, 79−91.
66. Kohwi, Y., and Kohwi-Shigematsu, T. (1988) *Proc. Natl. Acad. Sci. U.S.A. 85*, 3781−3785.
67. Völker, J., and Klump, H. H. (1994) *Biochemistry 33*, 13502−13508.
68. Roberts, R. W., and Crothers, D. M. (1996) *Proc. Natl. Acad. Sci. U.S.A. 93*, 4320−4325.
69. Roberts, R. W., and Crothers, D. M. (1992) *Science 258*, 1463−1466.

BI010666L